Phonon transport in hierarchically disordered Silicon nanostructures

D. Chakraborty*, S. Foster, L. de Sousa Oliveira, and N. Neophytou

I. Introduction

Roughly two thirds of all energy generated is lost as waste heat [1]. Thermoelectric power generation provides a means to convert this waste heat into useful energy. Yet conventional methods and materials typically provide only a low thermoelectric efficiency. Nanostructuring is a promising approach for next generation thermoelectric materials yielding ultra-low thermal conductivities and enhanced thermoelectric performance. More specifically, some of the lower thermal conductivities in nanocrystalline materials have been achieved in materials that include hierarchically sized structures scattering phonons of various wavelengths, thus reducing phonon transport throughout the spectrum [1]. Introduction of nanoporous structures referred to as 'holey' materials, allows for ultralow thermal conductivity- even below the amorphous limit [2]. Thus elaborate simulations, that can account for all nanostructured details are needed to understand heat transport.

II. Approach

In this work, we describe the development of a large scale, comprehensive Monte Carlo simulator to model thermal transport in nanostructured materials with a large and arbitrary degree of hierarchical disorder. Our simulations are based on the single phonon Monte Carlo algorithm to solve the Boltzmann Transport Equation for phonons, which provides high computational efficiency, as well as accuracy [3]. The phonons are initialized as per a 'single-phonon Monte Carlo' approach which differs from the multi-phonon Monte Carlo approach described in various works in the literature [4, 5]. In the single phonon approach one phonon is simulated at a time from the domain boundary/edge and propagates through the simulation domain until it exits at either edge. Once the phonon exits the next phonon is then initialized.

The polarization probability, frequency, velocity, and energy of each phonon is drawn from the dispersion relation $\omega(k)$, modified by the Bose Einstein distribution at the given temperature. The fit for the dispersion relation ω and the group velocity $\boldsymbol{v}_g$ is obtained as by Pop *et* al. [5] using equations 1 and 2 below.

$$\boldsymbol{\omega}(k) = v_s + ck^2 \tag{1}$$

$$\boldsymbol{v}_g = \frac{\mathrm{d}\omega}{\mathrm{d}k} \tag{2}$$

Phonons either scatter or are in free flight. Scattering of phonons is caused either by interaction with geometrical features or by three-phonon internal scattering (Umklapp processes). The three-phonon scattering, which is chiefly responsible for the change in temperature of the domain, is simulated in the relaxation time approximation and is a function of temperature and frequency. This is given as,

$$\tau_{\mathrm{TA,\,U}}^{-1} = \begin{cases} 0 & for\ \omega < \omega_{1/2} \\ \dfrac{B_{\mathrm{U}}^{\mathrm{TA}}\omega^2}{\sinh\left(\dfrac{\hbar\omega}{k_{\mathrm{B}}T}\right)} & for\ \omega > \omega_{1/2} \end{cases} \tag{3}$$

where ω is the frequency, T the temperature, the constant $B_{\mathrm{U}}^{\mathrm{TA}}$ = 5.5 × 10^{-18} s, and $\omega_{1/2}$ is the frequency corresponding to $k = k_{max}/2$ [6,7]. Repeated iterations and scattering events give a steady state thermal gradient as seen in Fig. 1.

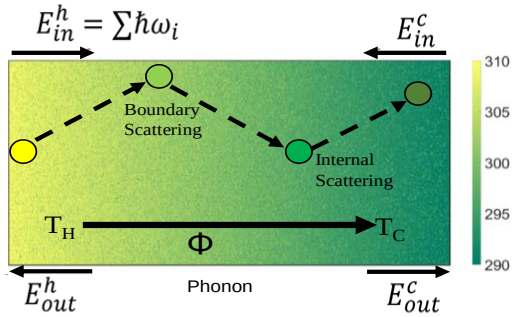

Fig. 1. Simulation scheme depicting a phonon initialized from the hot junction (T_H) propagating through the simulation domain undergoing internal (phonon-phonon) and boundary scattering and exiting the simulation domain to the right. The simulation domain here has the hot junction with a temperature set at 310 K (yellow) and a cold junction with a temperature of 290 K (green). 5 million phonons are inserted at both junctions and allowed to propagate through the simulation domain, and a thermal gradient is thus established. Comparing the energies of the phonons entering and exiting the simulation domain a phonon flux is obtained.

Considering the energy of the phonons entering (E_{in}^{h}, E_{in}^{c}) and leaving (E_{out}^{h}, E_{out}^{c}) the simulation domain from either side, an average phonon flux is determined which is used to extract the thermal conductivity. Thus, we do not extract thermal conductivity by computing the flux that crosses a particular cross section of the domain but by computing the net flux through the entire simulation domain. The finite size of the

Research supported by the European Research Council (ERC) under the European Union's Horizon 2020 Research and Innovation Programme (Grant Agreement No. 678763).

Dhritiman Chakraborty* (D.Chakraborty@warwick.ac.uk)
*Corresponding Author.

Samuel Foster (S.Foster@warwick.ac.uk)
Laura de Sousa Oliveira (L.de-sousa-oliveira@warwick.ac.uk)
Neophytos Neophytou (N.Neophytou@warwick.ac.uk)

Authors are with the school of Engineering, University of Warwick.

simulation domain is overcome by using the average mean-free-path to scale the simulated thermal conductivity to the actual thermal conductivity for an infinite channel length. This method makes much easier the book-keeping of all phonon attributes and could be more efficient in terms of memory requirements with the same accuracy as the more 'conventionally' used methods. We note that this approach is common in electronic transport Monte Carlo simulations, and we adopt it here for phonon transport [8, 9]. Geometry induced scattering of phonons on grain boundaries, surface boundaries, several defects, voids, and dislocations as in realistic nanocomposite which all contribute to reducing thermal conductivity, are investigated; always while keeping in mind that significant degree of crystallinity should be allowed to keep the electronic conductivity high. The effects of boundary roughness, porosity and disordered geometry are also examined. We believe that the code could play a very useful part in optimizing thermal conductivity reductions not only in Si-based materials, but in various other types of nanostructured materials in general.

III. Results

The simulator was validated for the bulk case. Structures like grain boundaries (seen in Fig.2 (a)) and nanoporous structures (as seen in Fig. 2 (c)) were considered where geometry induced scattering was observed.

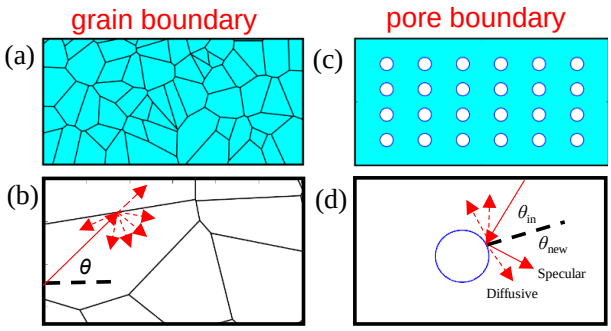

Figure 2. (a) Example of a typical nanocrystalline geometry simulated with average grain dimension <*d*> of 140 nm. (b) Schematic of the scattering mechanism for grain boundary scattering, indicating the initial angle of the phonon θ from the normal (black dashed line), grain boundaries (black lines), initial path of the phonon (red line) and probable paths of the phonon after scattering (red dashed lines). The probability of scattering is a function of the phonon wave vector, the roughness of the boundary Δ_{rms} and the angle of the phonon with the grain boundary θ_{GB}. (c) Example of a typical nanoporous geometry simulated, for an ordered rectangular case, with porosity of about 10%. (d) Schematic of scattering mechanism for pore scattering, indicating the pore boundary (blue line), the initial angle of the phonon θ_{in}, and potential new angle of propagation θ_{new} depending on specularity parameter *p*. Probable paths of the phonon after scattering for both diffusive (red dashed lines) and specular (red solid line) are also depicted. In the case of fully specular scattering, $p = 1$ and the phonon is reflected with a θ_{new} equal in magnitude to the initial angle θ_{in}. In the case of fully diffusive scattering $p = 0$.

Following this, more complex geometries were simulated giving reduced thermal conductivities. In the case of porous silicon nanomaterials it was verified that the effect of porosity is stronger than that of boundary roughness.

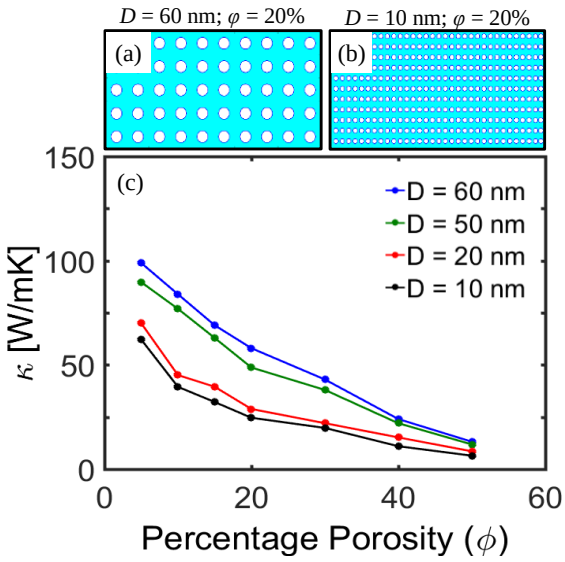

Figure 3. Effect of pore size and density on (κ) is examined. Here, a certain porosity, is achieved by utilizing pores of different sizes (D = 60 nm, 50 nm, 20 nm, and 10 nm depicted by the blue, green, red, and black lines, respectively). Typical geometries for a rectangular arrangement of pores giving the same porosity for different pore sizes D = 60 nm and D = 10 nm are depicted in (a) and (b) respectively. These are for a fixed specularity p = 0.1. It is observed that reduction in pore diameter leads to lower thermal conductivity at the same porosity. However, this effect diminishes as porosity increases.

We also show (in Fig. 3) that at the same porosity, a larger decrease in thermal conductivity is achieved by increasing pore number density than by increasing the pore diameter. An almost 50% decrease in thermal conductivity is observed with a decrease in pore diameter from D = 60 nm to D = 10 nm at the same porosity (observed for porosities from 15 % to 25%); however, this effect diminishes at higher porosities (φ = 35% and above). Our results would be useful in the design of nanostructured thermoelectric materials with ultra-low thermal conductivities.

References

[1] K. Biswas, J. He, I.D. Blum, C. Wu, T. P. Hogan, D. N. Seidman, V. P. Dravid, and M. G. Kanatzidis, Nature (2012): 489.7416: 414-18.

[2] J. A. P.-Taborda, M. M.-Rojo, J. Maiz, N. Neophytou, M. M. González, Nature Sci. Rep., (2016): 6, 32778.

[3] Wolf, S., Neophytou, N., Stanojevic, Z., & Kosina, H. (2014) Journal of electronic materials, 43(10), 3870-3875.

[4] Mazumder, Sandip, and Arunava Majumdar, Transactions-ASME Journal of Heat Transfer 123.4 (2001): 749-759.

[5] Pop, Eric, Robert W. Dutton, and Kenneth E. Goodson, Journal of Applied Physics 96.9 (2004): 4998-5005.

[6] Wolf, Stefanie, Neophytos Neophytou, and Hans Kosina. Journal of Applied Physics 115.20 (2014): 204306.

[7] Lacroix, David, Karl Joulain, and Denis Lemonnier. Physical Review B 72.6 (2005): 064305.

[8] Jacoboni, C., & Reggiani, L. Rev. Mod. Phys., (1983): 55(3), 645–705.

[9] Kosina, H., Nedjalkov, M., & Selberherr, S. IEEE (2000) Electron Devices, 47(10), 1898–1908.